Using High-Fidelity Computational Fluid Dynamics to Help Design a Wind Turbine Wake

Churchfield, Matthew J.; Wang, Qi ; Scholbrock, A.; Herges, T.; Mikkelsen, Torben Krogh; Sjöholm, Mikael

Published in:
Journal of Physics: Conference Series (Online)

Link to article, DOI:
10.1088/1742-6596/753/3/032009

Publication date:
2016

Using High-Fidelity Computational Fluid Dynamics to Help Design a Wind Turbine Wake Measurement Experiment

2016 J. Phys.: Conf. Ser. 753 032009

(http://iopscience.iop.org/1742-6596/753/3/032009)

Using High-Fidelity Computational Fluid Dynamics to Help Design a Wind Turbine Wake Measurement Experiment

M Churchfield[1], Q Wang[1], A Scholbrock[1], T Herges[2], T Mikkelsen[3] and M Sjöholm[3]

[1] National Renewable Energy Laboratory, Golden, Colorado, 80401 USA
[2] Sandia National Laboratories, Albuquerque, New Mexico, 87123 USA
[3] Technical University of Denmark, Roskilde, 4000 Denmark

E-mail: Matt.Churchfield@nrel.gov

Abstract. We describe the process of using large-eddy simulations of wind turbine wake flow to help design a wake measurement campaign. The main goal of the experiment is to measure wakes and wake deflection that result from intentional yaw misalignment under a variety of atmospheric conditions at the Scaled Wind Farm Technology facility operated by Sandia National Laboratories in Lubbock, Texas. Prior simulation studies have shown that wake deflection may be used for wind-plant control that maximizes plant power output. In this study, simulations are performed to characterize wake deflection and general behavior before the experiment is performed to ensure better upfront planning. Beyond characterizing the expected wake behavior, we also use the large-eddy simulation to test a virtual version of the lidar we plan to use to measure the wake and better understand our lidar scan strategy options. This work is an excellent example of a "simulation-in-the-loop" measurement campaign.

1. Introduction

Fluid flow simulations and experiments are often not well integrated. Commonly, experimental measurements are taken, and then the collected data are used to validate fluid flow models, such as computational fluid dynamics (CFD). Sometimes, however, fluid flow simulations and experiments are integrated such that computations are performed beforehand to inform the experiment, and experimental data are later used to validate and refine the computational method. This process can be iterative, and sometimes it is described as "simulation-in-the-loop."

We are using a simulation-in-the-loop process to help design a wind-turbine-wake measurement campaign. The experiment, which is described in detail in a companion paper by Fleming et al. [1], will take place at the Scaled Wind Farm Technology (SWiFT) facility located near Lubbock, Texas, and operated by Sandia National Laboratories [2]. It is composed of three Vestas V27 turbines that each have a rated power of 225 kW. Central to the experiment is the use of a scanning lidar to measure the wake. A main objective of the experiment is to measure the lateral wake deflection that occurs because of intentional rotor yaw misalignment. This wake deflection can be used in global wind power plant control systems that attempt to optimize the power production of the entire plant. When wind turbine wake effects decrease the

plant's efficiency, the wakes could be laterally deflected to minimize those effects and increase power production. This approach has been well documented in simulations by Jiménez et al. [3], Fleming et al. [4, 5], Churchfield et al. [6], and Howland et al. [7]. It has also been demonstrated in wind tunnel measurements by Campagnolo et al. [8, 9], Schottler et al. [10], and Howland et al. [7]. Wake deflection has not, however, been documented in the field on full-size turbines in real atmospheric flow.

In general, performing simulations before the experiment has helped provide a better understanding of what to expect when the experimental campaign begins. Specifically, the main objectives of these simulations are to:

- Quantify the expected mean wake deflection, shape, and deficit as a function of yaw-misalignment angle, downstream distance, and atmospheric inflow conditions;
- Quantify expected wake meandering behavior and how atmospheric conditions impact it;
- Test a virtual representation of the lidar to be used in the experiment to better understand the lidar's performance and how to mount it on the upstream turbine;
- Begin to form a work flow for processing and interpreting the experimental data.

2. Approach

For this work, we used the Simulator fOr Wind Farm Applications (SOWFA) [11] created by the National Renewable Energy Laboratory (NREL). SOWFA is a custom set of solvers, boundary conditions, and wind turbine aerodynamics models meant for performing wind plant large-eddy simulations (LES). It is built on the OpenFOAM CFD toolbox [12], so it uses the unstructured finite-volume formulation and is second-order accurate in time and space. The filtered, incompressible Navier-Stokes equations are solved including Coriolis and geostrophic forcing and with the Boussinesq approximation for buoyancy, which means that the temperature transport equation is also solved. The Lilly/Deardorff one-equation, subgrid-scale model is also solved. The inflow atmospheric turbulence is generated via horizontally periodic precursor atmospheric LES. A time series of inflow boundary data is generated by a precursor, and it is used as the inflow boundary conditions for the inflow/outflow wind plant simulation. The turbine is modeled using a rotating actuator line representation of the rotor. Thorough overviews of SOWFA and an example of validation of the solver are given in [13] and [14].

Atmospheric conditions at SWiFT are characterized from data collected by a meteorological tower located nearby. This characterization is documented by Kelley and Ennis [2], and then three representative atmospheric inflows are generated in the precursor step to match the site's characteristic conditions. These inflows all have the same mean hub-height wind speed and direction, but they are of slightly stable, neutral, and unstable stratification, which affects the resultant shear, veer, and turbulence level and structure as summarized in Table 1. All precursor simulations use a uniform 10-m grid resolution. Both the stable and neutral simulations use 3-km-by-3-km-by-1-km domain extents in the two horizontal and vertical directions, respectively. The unstable simulation uses a 4-km-by-7-km-by-1.8-km domain to fit the larger convective turbulent structures. The time required to fully develop the atmospheric boundary layer ranges from 7,000 s for unstable stratification to 30,000 s for neutral and stable stratification.

The precursor domain sizes are used for the respective wind plant simulations, but regions of successively refined mesh are included to capture the details of the rotor-local flow and the wake. The finest region around the rotor and wake has a resolution 31.25 cm, and it extends 6 rotor diameters (D) upstream of the rotor and 7D downstream. It also extends 1D to either side of the rotor centerline and 1D above the rotor hub. This results in roughly 80×10^6 mesh cells per wind plant simulation. Time steps are 0.02 s to well resolve the actuator line blade tip motion, and the overall simulations range from 700 s for the neutral and stable cases to 1300 s for the unstable cases. The first 100 s are discarded as they contain the wake's initial transient.

Table 1. A summary of the three atmospheric inflow conditions used in this study where Ri is Richardson number and L is Obukhov length.

Case	Surface Roughness (m)	Surface Temp. Flux (K-m/s)	H.H. Mean Wind Speed/Dir. (m/s / °)	H.H. Shear Exponent	H.H. Turbulence Intensity (%)	Bulk Ri	L (m)
Stable	0.01	-0.03	6.5/180	0.29	8.5	0.147	34.5
Neutral	0.01	0	6.5/180	0.14	10.7	0	∞
Unstable	0.01	0.1	6.5/180	0.06	17.2	-0.039	-40.1

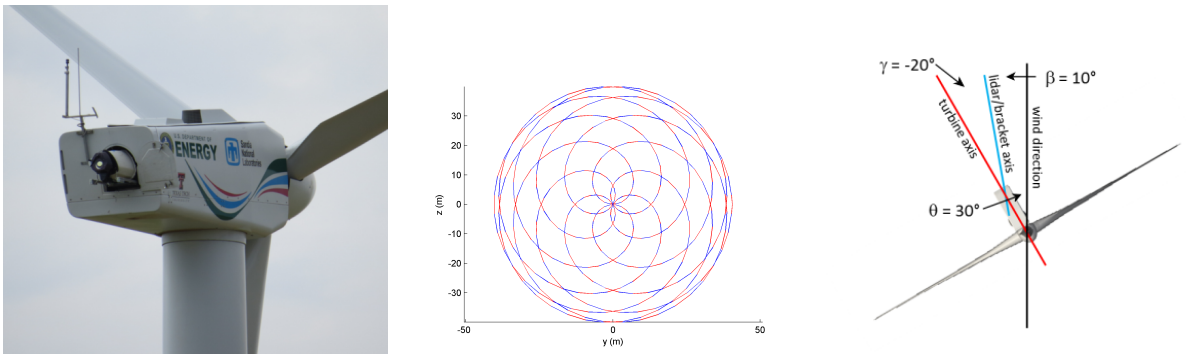

(a) (b) (c)

Figure 1. (a) The lidar installed in the nacelle of the SWiFT a1 turbine. (Photo by T. Herges, Sandia National Laboratories.) (b) The rosette scan pattern of the lidar. (c) The conventions and symbols used to describe yaw misalignment and lidar angle relative to the wind.

For each generated inflow, multiple simulations with the turbine included are performed. For example, for the stably stratified case, five different cases were run in which the yaw-misalignment angle was set between $-30°$ and $+30°$ in $15°$ increments. The resultant wake deflection trajectory and wake shape can be characterized from the collected data.

There is no one agreed-upon way to quantify the wake position and shape. Aitken et al. [15] and Machefaux et al. [16] present two different ways to identify wake location and shape based on fitting Gaussian-based profiles to the data. Doubrawa et al. [17] attempt to locate the wake edge by tracing out a specific velocity contour level and finding the geometric center of that contour shape. In this work, we follow Doubrawa et al. [17], but we choose the contour level to trace out in a different way. When looking at mean flow, we simply chose the contour that is at 50% of the maximum deficit and for instantaneous flow, we find that the 75% level is more robust.

The lidar used in the SWiFT field experiment will be the SpinnerLidar of the Technical University of Denmark (DTU), which is described by Mikkelsen et al. [18]. The lidar is rear-mounted on a manually swiveling bracket in the nacelle of the upstream turbine as shown in Figure 1(a). It is a continuous-wave, modified ZephIR lidar that uses a set of rotating prisms connected at a fixed gear ratio to trace out a rosette scan pattern as shown in Figure 1(b). It uses a focusing lens to perform scans at different distances. In our simulations, a model for the lidar is embedded so that we can compare an estimate of the lidar-sampled flow field to the pure LES data. At every time step in the simulation, the portion of the scan pattern corresponding to that time step is sampled and saved. A Lorentzian line-of-sight weighting function is applied to recover the line-of-sight velocity observed by the lidar. The angle conventions used to define the

yaw-misalignment angle and the lidar central angle relative to the nacelle and wind are shown in Figure 1(c). The right-hand rule about the positive z-axis (up) is used to define the turbine axis relative to the wind direction and the lidar/bracket axis relative to the turbine axis.

3. Results

3.1. Overview of the Flow

This section presents a qualitative overview of the results to provide a sense of the differences caused by the three different atmospheric inflows used in this study. The left pane of Figure 2 shows slices of instantaneous streamwise velocity in a hub-height horizontal plane for all three different inflows. The stable and neutral simulations required smaller domains; hence, their contour planes are smaller. The differences in turbulence structure of the inflow wind is clearly visible, with the stably stratified case having the finest grained structures. In the neutrally stratified case, the characteristic, streamwise-oriented, streaky low-speed turbulent structures are visible. In the unstably stratified case, the convection-driven turbulent structures are much larger than in the other two cases, which is why we used the larger simulation domain. In the left pane of the figures (Full Domain), the wake is barely visible within the yellow box. The right pane is the region of the contour plane within the yellow box enlarged so that the wakes are visible. The rotor location is denoted with a yellow cylinder. From this overview of the flow, we can already see that progressing from stable to unstable atmospheric stratification increases turbulence levels and therefore wake lateral meandering motion.

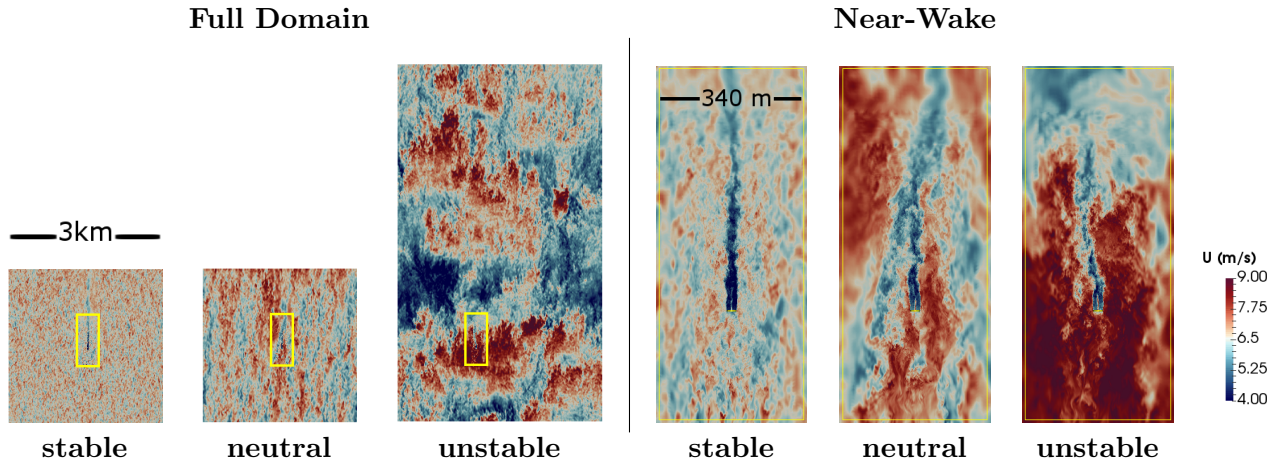

Figure 2. Contours of instantaneous streamwise velocity in a horizontal plane at the turbine hub height of 32.6 m for the three differently stratified inflow conditions. The left pane shows the entire domain (Full Domain). The right pane (Near-Wake) is a close-up view of the region around the turbine (shown as a yellow disk) and wakes. This region is outlined with a yellow box in the left-pane views for reference.

Figure 3 shows transverse vertical cuts through the computed wakes at 5D downstream for the stably stratified case. Here we plot contours of the instantaneous velocity minus the time averaged of the inflow velocity (i.e., the undisturbed mean wind speed and direction profile as a function of height). The wake deficit is clearly visible in blue. The white contour line is at 75% of the maximum deficit and nicely outlines the wakes' highly turbulent and irregular shape. Using the magenta outline of the projected rotor disk area, it is clear that with 30° of yaw misalignment, the wake is deflected in the positive y-direction. However, these static images cannot convey the highly unsteady nature of the computed wakes and how they meander laterally and vertically. All yaw-misalignment cases of a particular inflow type use the same realization of that inflow,

and this is apparent in Figure 3. Although the wake itself looks different when comparing the 0° yaw-misalignment case to the 30° case, the surrounding flow is similar.

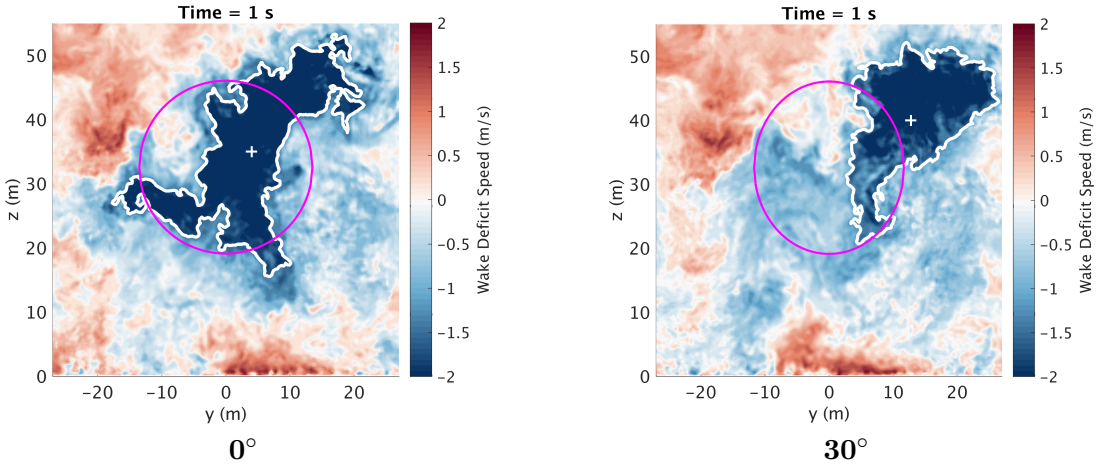

Figure 3. Contours of computed instantaneous streamwise velocity (the time-averaged inflow wind profile is subtracted) in vertical planes cutting through the wake at 5D downstream of the rotor for yaw-misalignment angles 0° and +30° for the case of inflow with stable atmospheric stratification. This data is viewed from the upstream looking toward the downstream. The magenta circle is the projected rotor area. The white contour line is set at 75% of the maximum deficit, and the white cross indicates the geometric center of the white contour line.

3.2. Mean Wake Behavior

One of the main purposes of this simulation campaign was to obtain an estimate of mean wake behavior in the SWiFT experimental campaign. Most importantly, we intend to gain an estimate of how much wake deflection to expect as a function of yaw misalignment, downstream distance, and inflow wind condition.

Figure 4 shows contours of computed time-averaged streamwise velocity (minus the inflow wind profile) in transverse vertical cuts through the wake at 1D, 3D, and 5D downstream for the neutrally stratified inflow case for a range of yaw misalignment angles. The time average is over 10 minutes. Here, a few things can be observed. First, the wake deficit decays with downstream distance, as expected. Next, we can clearly see that there is wake deflection, and that it increases as yaw misalignment and distance downstream increase. We see that as the yaw misalignment increases, the wake increasingly deflects and its maximum deficit decreases, which is a byproduct of the decreased axial thrust imparted on the flow by the turbine. As the yaw misalignment angle increases, the rotor frontal area decreases, the thrust vector is not completely pointed into the wind, and the rotor extracts less energy from the flow, all of which theoretically decrease the axial thrust on the flow. Last, we see that with large yaw misalignment angles, the wake develops kidney-shaped contours.

To better quantify how wake deflection changes as a function of yaw-misalignment angle, we plot mean lateral wake deflection at 5D downstream from the case with neutrally stratified inflow in Figure 5. We define the deflection by tracing out the contour level that lies at 50% of the maximum mean wake deficit and defining the wake location as the geometric center of the shape traced out by the contour. We can see that between −20° and +20° of yaw misalignment, the lateral deflection responds nearly linearly. Beyond ±20°, the deflection effect diminishes, likely because the rotor thrust is diminishing. We see that at this distance downstream, at best,

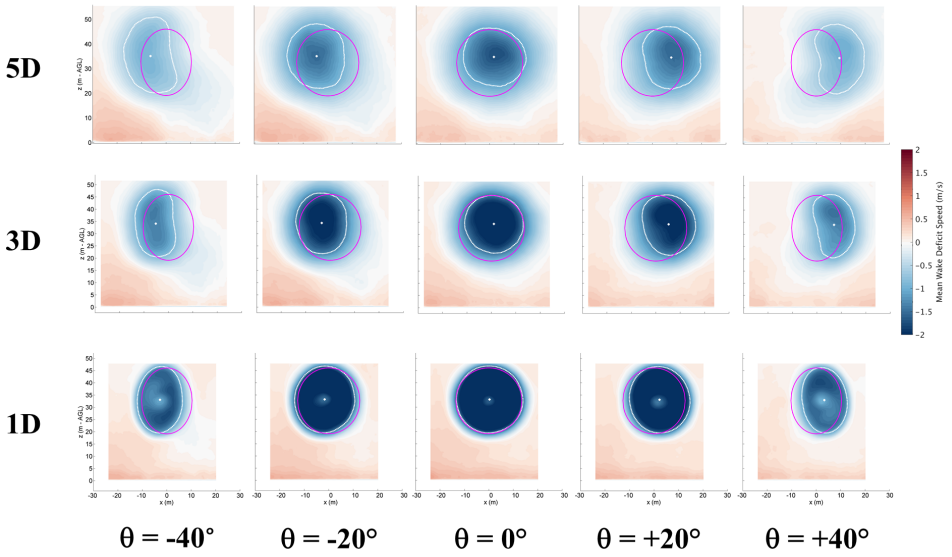

Figure 4. Contours of computed mean streamwise velocity (the mean inflow shear is subtracted) in vertical planes cutting through the wake at 1D, 3D, and 5D downstream of the rotor for yaw misalignment angles ranging from $-40°$ to $+40°$ for the case of inflow with neutral atmospheric stratification. This data is viewed from the upstream looking toward the downstream.

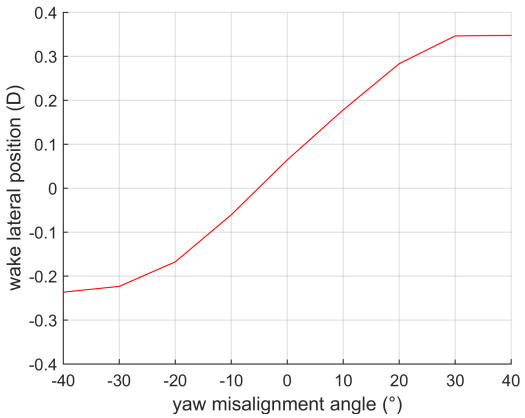

Figure 5. Mean lateral wake deflection for the case with neutrally stratified inflow at 5D downstream.

yaw misalignment laterally moves the wake about one-third of a rotor diameter. Although that number may not seem large, the implications for increased power production on a downstream turbine is very significant.

To quantify both the effect of atmospheric stability and downstream distance on wake deflection, we plot computed mean lateral wake deflection as a function of downstream distance in Figure 6 for both the stably (blue) and unstably (red) stratified inflows, bracketing the range of inflow turbulence levels. We only show wake deflection for the $-30°$, $0°$, and $+30°$ yaw-misalignment settings. In Figure 6(a), the lateral deflection as measured from the LES results is shown. The unstably stratified case clearly has a bias to the left. Upon further inspection of the inflow, we see that a large turbulent structure with a mean lateral flow component passes over

the turbine during the averaging time period. That structure carries the wake to the left. The stably stratified case has a less pronounced bias to the right, which is caused by a combination of factors. First, the combination of increased vertical wind speed shear of the inflow and wake rotation causes the maximum deficit of the wake to first appear at the bottom of the wake, and then that maximum deficit rotates to the right side of the wake (as viewed from above and looking downstream). Second, the significant wind direction veer in the stably stratified case skews the wake, which may add to the bias to the right of the wake location. To remove these biases caused by the inflow, we subtract the zero yaw-misalignment deflection values from the nonzero values, which is shown in Figure 6(b). In that figure, we can clearly see that the wake deflection increases with increasing downstream distance, but the increase is not linear; it decays with distance. This agrees well with the simulations and wake deflection model of Jimenez et al. [3]. The more important conclusion, though, is that under unstably stratified atmospheric conditions, the wake deflection is decreased. This is likely caused by the fact that the turbulence level is much higher in this case than the stably stratified case.

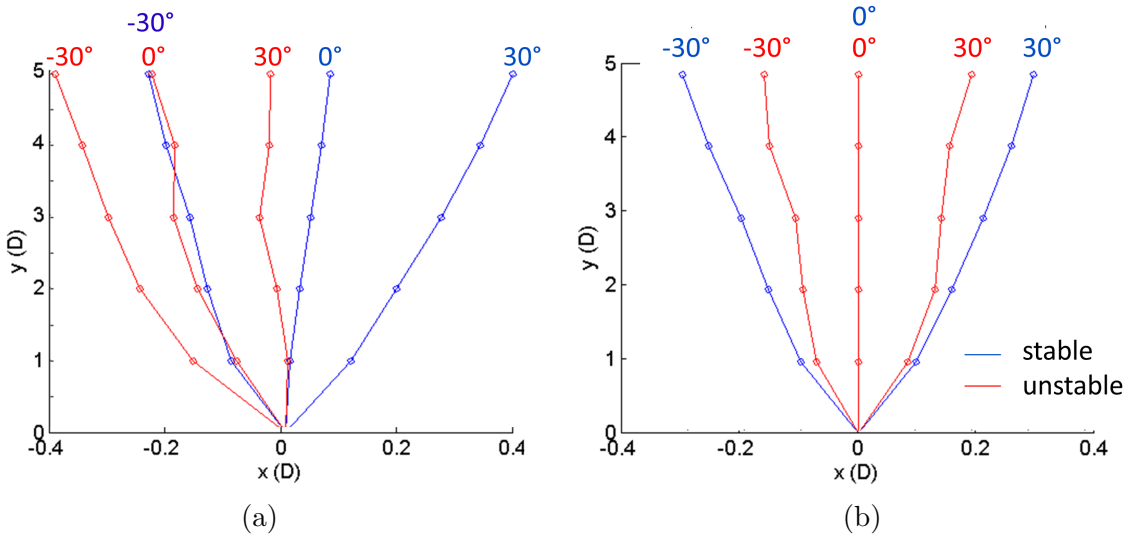

Figure 6. Computed mean lateral wake deflection as a function of downstream distance for the stably and unstably stratified atmospheric inflow cases and for different yaw angles. Plot (a) shows the wake deflection directly measured from the simulation data, and plot (b) subtracts the 0° yaw-misalignment deflection from the ±30° yaw-misalignment case.

3.3. Virtual Lidar Performance

In this section, we show the results of sampling the LES flow field with the virtual DTU SpinnerLidar. Because we are predominantly interested in the time-averaged behavior of wake deflection, we begin by comparing the LES-computed, time-averaged wake flow field with the time-averaged, virtual lidar sampling of the LES-computed wake in Figure 7. In this figure, we show contours of the streamwise wake velocity (minus the mean inflow profile) in a transverse slice at 5D downstream for both the stably and unstably stratified inflow situations for the +30° yaw-misalignment case. To go from the measured rosette pattern to the two-dimensional contour plot, Matlab's griddata function is used. That function takes the irregular rosette point data set and uses Delauney triangulation to change it into a set of interlocking triangles that create a two-dimensional plane. Using the velocity data at each triangle's vertices, a linear, two-dimensional interpolation function can be defined within each triangle's area. That set of

interpolation functions is used to interpolate to a regular grid of points convenient for plotting. To compute the streamwise velocity, we divide the line-of-sight velocity that the lidar measures by the cosine of the angle between the beam and the downstream direction. We trace out the closed contour of velocity that is at 50% of the maximum velocity deficit along with that shape's geometric center so that we can visually assess the lidar's ability to detect wake shape and position. We show the contour at 5D downstream, both because that is the location of the second turbine at the SWiFT site, which will encounter the wake and benefit from yaw-based control, and because the lidar resolution is degraded here. It is degraded because the scan pattern widens with scan distance, increasing the distance between rosette "petals." In addition, the lidar line-of-sight weighting function becomes longer the further out it scans.

In Figure 7, if we first focus on the stably stratified inflow situation, we see that the virtual lidar captures the characteristics of the LES flow data reasonably well from which it is sampled. Most importantly, the mean deflection to the right is captured. The kidney shape of the deflected mean wake is also captured. The virtual lidar, though, does not capture the maximum deficit of the wake nor the extent of this deficit. This is caused both by the lack of resolution of sampling points (distance between rosette "petals" is large) and the fact that the Lorentzian line-of-sight lidar weighting function smooths the sampled data. This is an important consideration when validating computational models against lidar data. The actual lidar field measurements will be further complicated by issues such as variable lidar backscatter and nacelle motion noise. Without a clear understanding of how the lidar samples the flow field, it can be wrongly concluded that the computational data is not in agreement with the measured data. Ideally, a model for the measurement system should be applied to the computed data before comparing it with the measured data.

Next, if we examine the unstably stratified inflow situation data, we see that at 5D downstream the wake strength is much less than that of the stably stratified situation. This makes wake identification difficult even directly from the mean LES data. We can see that the wake location identified directly from the LES data differs from that of the virtual lidar sampling of that LES data, but the overall wide shape of the wake is captured. The main point is that the unstably stratified situation, especially at 5D and beyond, will be difficult to measure with the real lidar in the SWiFT experiment.

Measuring the mean behavior of the wake is our primary objective in the SWiFT experiment, but a secondary objective is to measure unsteady wake meandering behavior. In Figure 8, we show the virtual lidar's ability to capture instantaneous wake behavior. This figure is analogous to Figure 7, but shows instantaneous wake velocity contours. The stably stratified situation is in the top row and the unstably stratified situation is in the bottom row. Interestingly, even with the lack of resolution, the virtual lidar sampling of the LES flow field maintains the main larger-scale flow structures. The instantaneous wake location and main features of the shape are captured. The steep gradients seen in the contours directly taken from the LES data, though, are not captured when applying the lidar sampling and weighting function.

To better quantify the lidar's ability to track wake meandering, we plot lateral wake motion in Figure 9. The motion is quantified using the geometric center of the 75% of maximum deficit contour shape method. We show results for the stably stratified situation at 3D and 5D downstream, and we compare tracking the wake motion directly from the LES data to that from the virtual lidar sampling of the same LES data. The root-mean-square error between the virtual lidar and straight LES wake location roughly doubles when going from 3D to 5D.

3.4. Data Averaging Considerations

Because of the inflow variability is a function of atmospheric stability, we expect that different amounts of averaging time will be necessary to compute converged statistics about the wakes depending on the inflow atmospheric stability. These simulations have helped us better

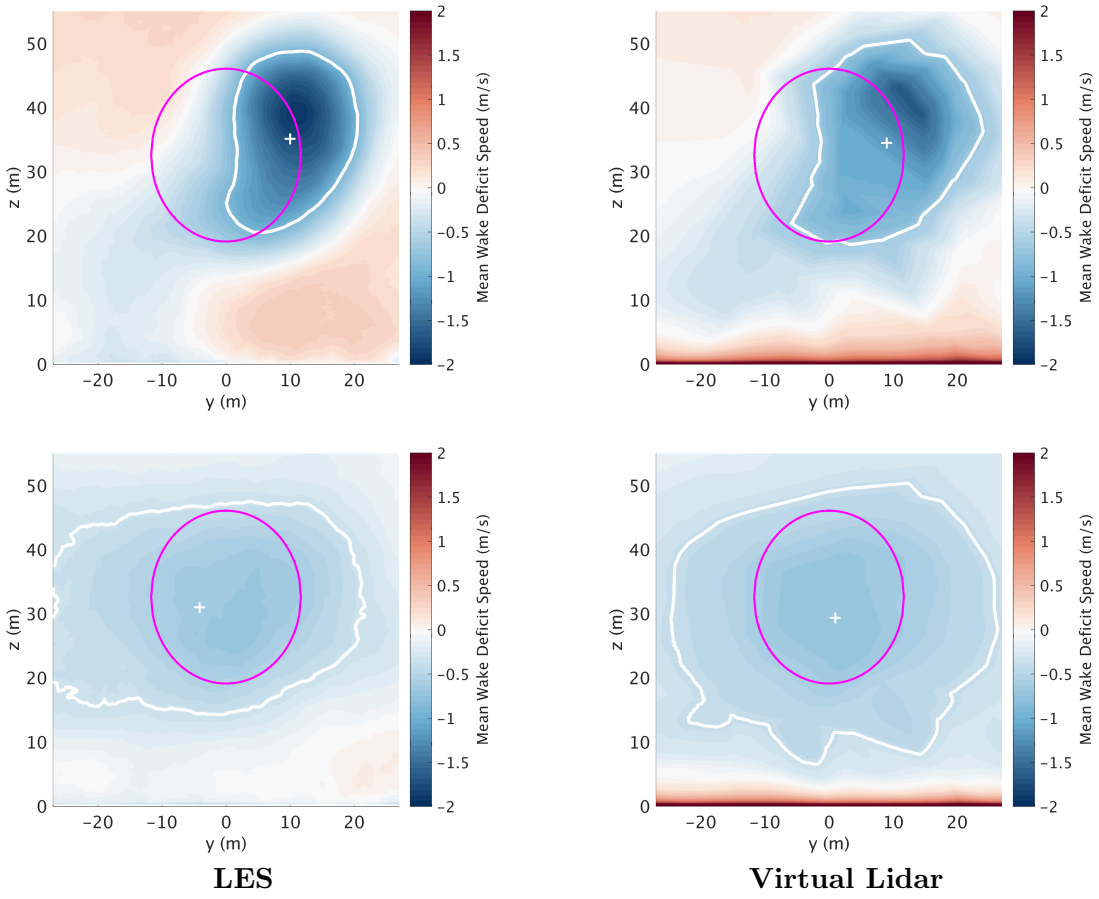

Figure 7. Contours of mean streamwise velocity (the mean inflow shear is subtracted) in vertical planes cutting through the wake at 5D downstream of the rotor for a yaw-misalignment angle of $+30°$ for the case of inflow with stable (top row) and unstable (bottom row) atmospheric stratification. The first column (LES) shows contours taken directly from the LES data; the second column (Virtual Lidar) depicts from the virtual lidar embedded in the same LES. This data is viewed from the upstream looking toward the downstream. The white contour line is set at 50% of the maximum deficit, and the white cross indicates the geometric center of the white contour line.

understand the averaging times required. For example, Figure 10 shows the convergence of the mean wake velocity in a plane 5D downstream for the 30° yaw-misalignment case. It compares how the mean converges for the unstably and stably stratified conditions. As time increases at each point in the 5D sampling plane the mean is computed. We then compute the difference between the estimate of the mean at time n and time $n-1$ at every point in the plane. We then turn that distribution in change in mean at time n into a global quantity by taking the root-mean-square of all the values over the plane. Figure 10 is the time history of this root-mean-square evolution of the change in mean estimate, so it should converge towards zero as the estimate of the mean converges. We see that after 10 minutes, the mean wake velocity estimate is quite well converged in the stably stratified case. It takes roughly double that time for the mean to converge to the same level in the unstably stratified case.

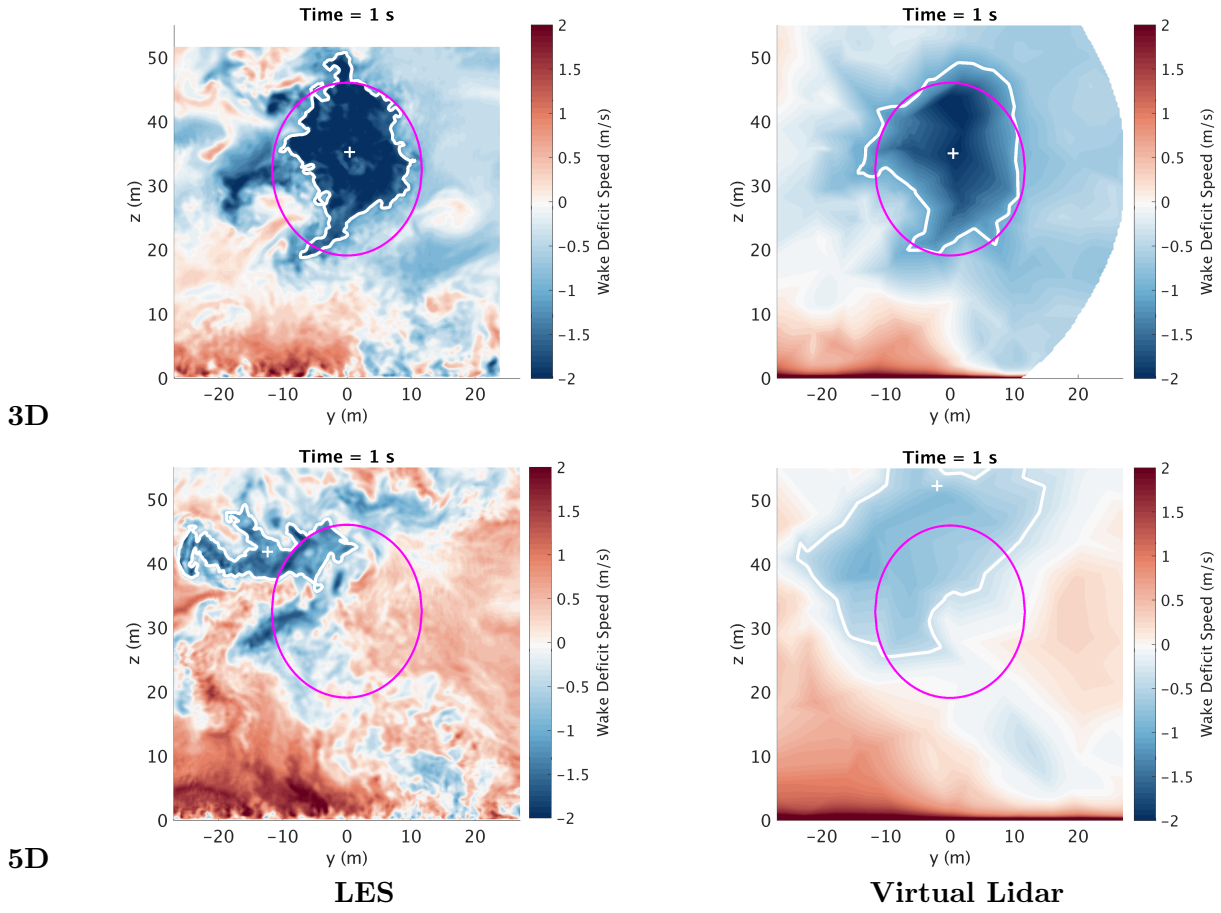

Figure 8. Contours of instantaneous streamwise velocity (the mean inflow shear is subtracted) in vertical planes cutting through the wake at 3D and 5D downstream of the rotor for a yaw misalignment angle of +30° for the case of inflow with unstable atmospheric stratification. The first column shows contours taken directly from the LES data; the second column shows contours provided by the virtual lidar embedded in the same LES. This data is viewed from the upstream looking toward the downstream.

4. Discussion and Conclusions

This simulation campaign, which was conducted in advance of the experimental campaign at the SWiFT facility and was intended to characterize wake behavior caused by yaw misalignment, has proven extremely useful. We gained an estimate of how the wake will behave under various levels of intentional rotor yaw misalignment and different atmospheric inflow conditions. We expect that wake deflection authority will be strongest under stably to neutrally stratified conditions, but the enhanced mixing of the convective, unstably stratified atmosphere decreases the amount of expected deflection. Under stable and neutral conditions, we expect a maximum wake deflection of roughly one-third of a rotor diameter at 5D downstream with 20° of yaw misalignment. For unstable inflow conditions, that deflection drops by roughly half.

Because of the increased variability of the inflow, we expected that unstably stratified inflow conditions characteristic of the daytime would be the most difficult to measure. Indeed, through these simulations, we found that it takes roughly double the amount of averaging time for the unstable case' mean to converge to the same level as that of the stable stratified case. We think that around 10 minutes of data provides converged statistics for the stably stratified case

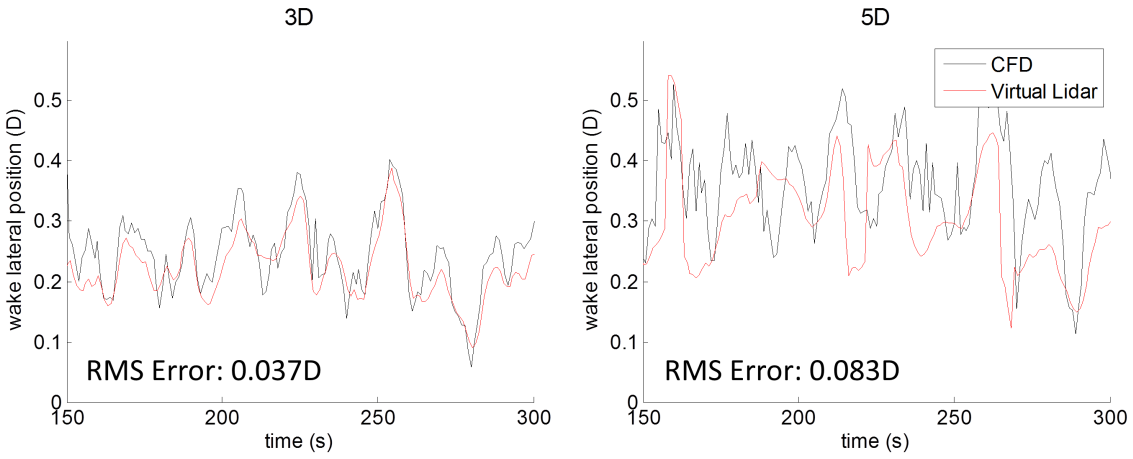

Figure 9. Plots of the time history of lateral wake motion from the stable case with 30° of yaw misalignment at 3D and 5D downstream. The motion obtained directly from the LES data is compared to that obtained using the virtual lidar embedded in the LES.

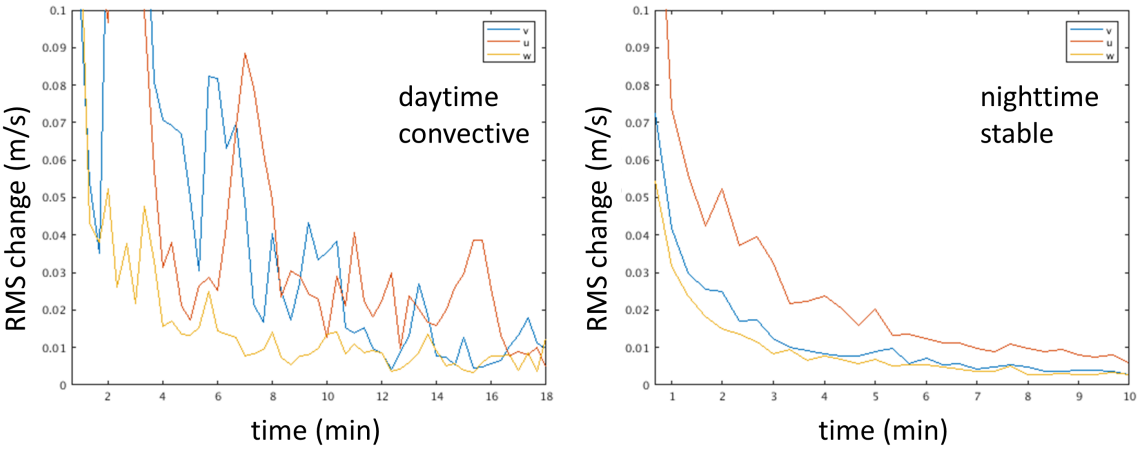

Figure 10. Plots of global convergence of the mean of the velocity in the wake as a function of averaging time. These plots compare the unstably stratified (left) to the stably stratified (right) conditions.

and 20 minutes of data are required for the unstably stratified case. This characterization of averaging time required to obtain converged statistics helps us form target values for the amount of continuous experimental data needed under different conditions to obtain converged statistics.

The mean wake deficit at 5D is quite weak, making wake deflection difficult to measure. In fact for the unstably stratified case, at times our ability to find the wake location becomes questionable. We observed simulated turbulent atmospheric flow structures that have the velocity deficit magnitude and shape similar to the wake, making instantaneous wake position identification difficult.

We have also characterized the ability of the DTU SpinnerLidar to capture the essential wake features of shape and position, both instantaneously and in the time average. The virtual modeled lidar does surprisingly well at capturing the wake position and shape both instantaneously and in the mean. Because of its resolution, the fine-scale details and steep gradients of the instantaneous wake are lost, but the overall shape is captured. Our work

in modeling the DTU SpinnerLidar has also illustrated that when comparing computational results to lidar data, one must fully understand how the lidar resolution and optics affect the measurements. We found that applying the line-of-sight Lorentzian weighting function to the LES data sampled in the lidar's rosette pattern is very important, especially at further downstream locations. It causes the wake deficit to appear weaker than it really is. Without taking computed data and applying the lidar transfer function to it, one could wrongly conclude that the computational model is overpredicting the wake deficit.

We also used these simulations to help design the lidar-mounting bracket that is described in a companion paper by Fleming et al. [1]. We found that the lidar central axis should not be separated from the wind direction by more than 20° or else it cannot fully capture the wake. The manually adjustable bracket was designed to account for this. We now know that for a test segment in which we are testing yaw-misalignment angles between 0° and 30°, we can set the bracket angle to 15° and feel confident that the lidar will be able to capture the wake.

Processing the simulated data has forced us to think much more about the work flow needed to process the experimental data when it begins to become available. For example, it has made us think about how to use the upstream meteorological tower data to subtract the inflow profile from the wake data to better isolate the wake flow. It has helped us explore various ways of characterizing wake position, something that we continue to develop.

Finally, because LES data are at a much finer resolution than measured data, it will help us to explain measured phenomena. For example, the virtual lidar is able to detect the kidney-shaped deflected wake, but it does not provide enough information to describe why that shape occurs. The full LES data allows us to see that with wake deflection, the rotor trails a pair of streamwise, counter-rotating vortices that induce flow on the wake, distorting its shape. These vortices form under the same principle that a helicopter rotor trails a pair of vortices—the rotor thrust vector now has a component perpendicular to the flow so it becomes a weakly sideways lifting body.

Acknowledgments

This work was supported by the U.S. Department of Energy under Contract No. DE-AC36-08GO28308 with the National Renewable Energy Laboratory. Funding for the work was provided by the DOE Office of Energy Efficiency and Renewable Energy, Wind and Water Power Technologies Office. This work was also conducted under Contract No. DE-AC04-94AL85000 with Sandia National Laboratories. The various members of the SWiFT experimental team have provided invaluable feedback about these simulations. In particular, Scott Schreck, Paul Fleming, and Brian Naughton have all helped define the simulation scope and actively used the results to help inform the experimental design.

References

[1] Fleming P, Churchfield M, Scholbrock A, Clifton A, Schreck S, Johnson K, Wright A, Gebraad P, Naughton B, Berg J, Herges T, White J, Mikkelsen T, Sjöholm M and Angelou N 2016 *The Science of Making Wind From Torque, Munich, Germany, Oct. 5–7, 2016*

[2] Kelley C L and Ennis B L 2016 SWiFT site atmospheric conditions Tech. Rep. SAND2016-0216 Sandia National Laboratories

[3] Jiménez Á, Crespo A and Migoya E 2010 *Wind Energy* **13** 559–572

[4] Fleming P A, Gebraad P M O, Lee S, van Wingerden J W, Johnson K, Churchfield M, Michalakes J, Spalart P and Moriarty P 2014 *Renewable Energy* **70** 211–218

[5] Fleming P A, Gebraad P M O, Lee S, van Wingerden J W, Johnson K, Churchfield M, Michalakes J, Spalart P and Moriarty P 2015 *Wind Energy* **18** 2135–2143
[6] Churchfield M J, Fleming P A, Bulder B and White S M 2015 *Offshore Technology Conference, Houston, TX, May 4–7, 2015* (Offshore Technology Conference) OTC-25644-MS
[7] Howland M F, Bossuyt J, Martínez-Tossas L A, Meyers J and Meneveau C 2016 Wake structure of wind turbines in yaw under uniform inflow conditions submitted to the Journal of Renewable and Sustainable Energy
[8] Campagnolo F, Petrovic V, Manos E M, Tan C W, Bottasso C L, Paek I, Kim H and Kim K 2016 *American Control Conference, Boston, MA, USA, Jul. 6–8, 2016*
[9] Campagnolo F, Petrovic V, Bottasso C L and Croce A 2016 *The 26th International Ocean and Polar Engineering Conference, Rhodes, Greece, Jun. 26– Jul. 1, 2016*
[10] Schottler J, Hölling A, Peinke J and Hölling M 2016 *34th Wind Energy Symposium, AIAA SciTech, San Diego, CA, USA Jan. 4–8, 2016* (AIAA, Washington D.C.) AIAA Paper 2016-1523
[11] Churchfield M and Lee S Simulator for wind farm applications (SOWFA) available online at http://wind.nrel.gov/designcodes/simulators/sowfa, accessed February 26, 2016 created by National Renewable Energy Laboratory
[12] OpenCFD Ltd (ESI Group) OPENFOAM – The open source CFD toolbox available online at http://www.openfoam.com, accessed February 26, 2016
[13] Churchfield M J, Lee S, Michalakes J and Moriarty P J 2012 *Journal of Turbulence* **13**
[14] Churchfield M J, Lee S, Moriarty P J, Martínez L A, Leonardi S, Vijayakumar G and Brasseur J G 2012 *50th AIAA Aerospace Sciences Meeting including the New Horizons Forum and Aerospace Exposition, Nashville, TN, USA Jan. 9–12, 2012* (AIAA, Washington D.C.) AIAA Paper 2012-537
[15] Aitken M L, Banta R M, Pichugina Y L and Lundquist J K 2014 *Journal of Atmospheric and Oceanic Technology* **31** 765–787
[16] Machefaux E, Larsen G C, Koblitz T, Troldborg N, Kelly M C, Chougule A, Hansen K S and Rodrigo J S 2015 *Wind Energy* Published online in Wiley Online Library DOI: 10.1002/we.1950
[17] Doubrawa P, Barthelmie R J, Wang H and Churchfield M J 2016 *The Science of Making Wind From Torque, Munich, Germany, Oct. 5–7, 2016*
[18] Mikkelsen T, Angelou N, Hansen K, Sjöholm M, Harris M, Slinger C, Hadley P, Scullion R, Ellis G and Vives G 2013 *Wind Energy* **16** 625–643